Micron 133 (2020) 102861

Contents lists available at ScienceDirect

Micron

journal homepage: www.elsevier.com/locate/micron

Computational fluid dynamics simulation from microCT stacks of commercial biomaterials usable for bone grafting

Daniel Chappard[a,*], Jean-Daniel Kün-Darbois[a,b], Bernard Guillaume[a,c]

[a] Groupe Etudes Remodelage Osseux et bioMatériaux, GEROM, LabCom nextBone, SFR-4208, Univ-Angers, IRIS-IBS Institut de Biologie en Santé, CHU-Angers, 49933 Angers, France
[b] Service de chirurgie maxillo-faciale, CHU d'Angers, 49933 Angers Cedex, France
[c] CFI, Collège Français d'Implantologie, 6 rue de Rome, 75005 Paris, France

ARTICLE INFO

Keywords:
Bone graft
Permeation
microCT
Computational fluid dynamics
Microarchitecture
Fluid flow

ABSTRACT

Granules of calcium/phosphate biomaterials are used to fill small bone defects in oral and maxilla-facial surgery. Granules of natural (e.g., trabecular bone, coral) or synthetic biomaterials are provided by industry. Small granules can also form of putty. The 3D geometry of granules creates a macroporosity allowing invasion of vascular and bone cells when pores are larger than 300 µm. We analyzed the 3D-porosity of 11 different stacks of biomaterials: Osteopure®, CopiOs®, Bio-Oss®, TCP Dental HP®, KeraOs®, TCH®, Biocoral®, EthOss® and Nanostim®. For each granular biomaterial, two sizes of granules were analyzed: small and large. Microcomputed tomography (microCT) determined porosity and microarchitectural characteristics of the biomaterials stacks. Computational fluid dynamics (CFD), a simulation method, was used on the stacks of microCT images.

Stacks of small granules had a much lower permeation and fluid velocity than large granules and the hydraulic tortuosity was increased. Significant correlations were observed between microarchitecture parameters (porosity, mean pore diameter and specific surface) and fluid dynamic parameters. The two putties were associated with low (or absence of) porosity and permeation study revealed a very low (or absence) of flow rate. Stacks of granules represent 3D scaffolds resembling trabecular bone with an interconnected porous microarchitecture. Small granules create pores less than 300 µm in diameter; this induces a low fluid flow rate. CFD simulates the accessibility of body fluids and progenitor cells and confirms that it is depending on the shape and 3D arrangements of granules within a stack. Large granules must be preferred to putties and small granules.

1. Introduction

Biomaterials in a granular form represent a common method for filling bone defects in oral - maxilla-facial surgery and orthopedics (Bohner, 2010b; Guillaume, 2017; Hernigou et al., 2017). However, there is now no real consensus in the literature and routine surgical technique concerning the nature and the modality of using and preparing such biomaterials. Industrial companies can provide biomaterials either synthetic or natural with various granulometry. The commonest presentations are represented by large granules (e.g., 1000 − 2000 µm), small granules (e.g., 250 − 1000 µm) and powder or pasty formulations (i.e., ready-to-use powder with a binding agent giving a putty with consistence similar to a toothpaste). Reports concerning these different forms exist in the literature but they are usually limited to a few clinical cases, especially in odontology journals. Although the chemical nature of the biomaterial appears of the upmost importance to ensure bone healing, it is likely that the shape of the granules and their 3D geometrical arrangement in the grafted site play a considerable role to favor cell colonization (Karageorgiou and Kaplan, 2005; Knabe et al., 2008; Lapczyna et al., 2014; Ndiaye et al., 2015).

When surgeons place granules within a bone cavitary defect, the voids between the granules represent an interconnected space available for bone cells to invade the grafted area (Carvalho et al., 2007; Guillaume, 2017; Redondo et al., 1995). The 3D geometry of these scaffolds has been little considered and depends on a number of factors such as the size and shape of the granules themselves. An open porosity with a high degree of interconnectivity and a pore size > 300 µm is now considered a key factor ensuring a rapid healing of the grafted site and the rapid colonization by vascular sprouts (Karageorgiou and Kaplan, 2005; Mastrogiacomo et al., 2006).

X-ray microcomputed tomography (microCT) is a powerful tool to analyze and measure the 3D volume, porosity and microarchitecture of

* Corresponding author at: GEROM, IRIS-IBS Institut de Biologie en Santé, Université d'Angers, CHU d'Angers, 49933 Angers Cedex, France.
E-mail address: daniel.chappard@univ-angers.fr (D. Chappard).

https://doi.org/10.1016/j.micron.2020.102861
Received 3 February 2020; Received in revised form 27 February 2020; Accepted 28 February 2020
Available online 29 February 2020
0968-4328/

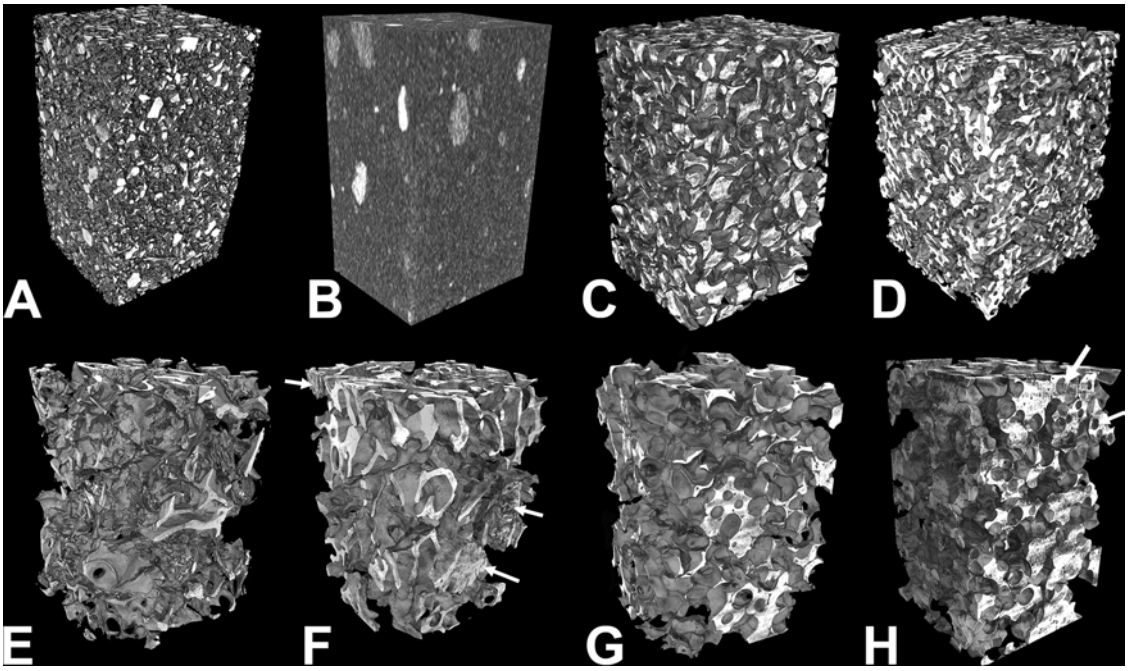

Fig. 1. MicroCT analysis of some biomaterials used in the present study. A) EthOss® is a powder composed of mineral particles packed together in a dry state. B) Nanostim® is a paste made of nanoparticles of hydroxyapatite in water. The paste is not homogeneous, and the nanoparticles tend to agglomerate in ill-defined areas that appear white in microCT. C) TCP Dental HP® in small granules closely packed together. D) Biocoral® granules. E) Osteopure® composed of large granules where whole trabeculae are clearly identified. F) Bio-Oss® appeared composed of a mixture of trabeculae and cortical bone fragments (arrows) identified by their compact aspect and presence of Haversian canals. G) TCP Dental HP® in large granules forming a scaffold with an interconnected porosity resembling trabecular bone microarchitecture. Compare with the smaller granules in C). H) KeraOs ® producing a porous scaffold; note that small round holes inside some granules represent a closed porosity (arrows).

Table 1
morphometric parameters obtained by microCT on the different stacks of granules.

	Porosity (Po in %)	Po.Diam (in µm)	Po.S/TV (mm^2/mm^3)
Powder/putty			
EthOss®	61.3 ± 2.0	39.9 ± 4.0	25.7 ± 1.7
Nanostim®	0.66 ± 0.3	6.08 ± 1.6	1.8 ± 0.6
< 1000 µm			
Osteopure®	76.7 ± 0.8	147 ± 9	8.67 ± 0.48
CopiOs®	65.3 ± 1.9	105 ± 7	10.31 ± 0.41
Bio-Oss®	57.9 ± 0.6	95 ± 7	10.16 ± 0.79
TCP Dental HP®	60.5 ± 2.4	94 ± 19	10.92 ± 1.84
KeraOs®	59.3 ± 0.7	111 ± 2	8.83 ± 0.25
TCH®	60.3 ± 0.3	110 ± 2	9.10 ± 0.17
Biocoral®	65.8 ± 1.3	112 ± 5	9.78 ± 0.5
1000 − 2000 µm			
Osteopure®	82.2 ± 0.1	252 ± 6	5.43 ± 0.12
Copios®	82.4 ± 1.9	314 ± 44	4.41 ± 0.55
Bio-Oss®	69.9 ± 1.7	226 ± 7	5.15 ± 0.05
TCP Dental HP®	79.4 ± 1.7	232 ± 8	5.69 ± 0.11
KeraOs®	63.0 ± 1.9	193 ± 14	5.44 ± 0.24
TCH®	63.7 ± 0.5	189 ± 7	5.61 ± 1.61

granule-based scaffolds *in vitro* (Farber et al., 2003; Ndiaye et al., 2015; van Lenthe et al., 2007v). Evaluation of the volumetric and micro-architectural parameters of the granule scaffolds is especially important to have a precise idea of their microarchitecture when they will be implanted in a bone defect. This is based on the assumption that the scaffolds represent a microarchitecture close to that of natural bone (Arbez et al., 2019; Arbez and Libouban, 2017; Chappard et al., 2015; N'Diaye et al., 2013; Tanaka et al., 2017). Trabecular bone consist of a macroporous scaffold of trabeculae made of an organic phase (mainly type I collagen) re-enforced with a mineral phase (carbonated hydroxyapatite). Measurement of bone volume in normal and osteoporotic patient bone samples revealed that it varies from ~11 to 30 % depending on the age and site analyzed (Ibrahim et al., 2013; Kim et al., 2015; Turunen et al., 2013). A large number of authors have used microCT to evaluated bone volume (and porosity is defined as 100- bone volume) (Blok et al., 2013; Chappard et al., 2008).

When applied to biomaterials, microCT allows a qualitative and quantitative analysis of the granule scaffolds but only indirect information can be obtained concerning their behavior via extracellular fluids. The permeability of virtual 3D models derived from microCT analysis can now be evaluated by means of numerical methods (Ochoa et al., 2009; Syahrom et al., 2013). These methods simulate the flow of a liquid through a stack of granules and different parameters can be determined and visualized graphically such as pressure, absolute permeability, tortuosity (i.e. complexity of the flow path).

This study aims i) to evaluate by microCT the 3D microarchitectures of different granular biomaterials prepared and sold by several companies ii) to determine the permeability parameters of the different stacks of granules. Investigating the transport of extracellular fluids through such stacks of granules by computer simulation is of paramount importance to appreciate their behavior when they will be used after grafting in a patient. Allogenic and xenogeneic particles and synthetic Ca/P ceramic granules commonly used in bone surgery were analyzed. The influence of two size of granules sold by industry (i.e., < 1000 µm and 1000 − 2000 µm) and the use of powder or putty was considered on the 3D microarchitecture and permeation analysis.

2. Material and methods

2.1. Biomaterial granules

2.1.1. Osteopure ® undecalcified human graft

A hemi-femoral head (Osteopure ®) was provided by Ost Development (France). The sample did not contain cortical bone and

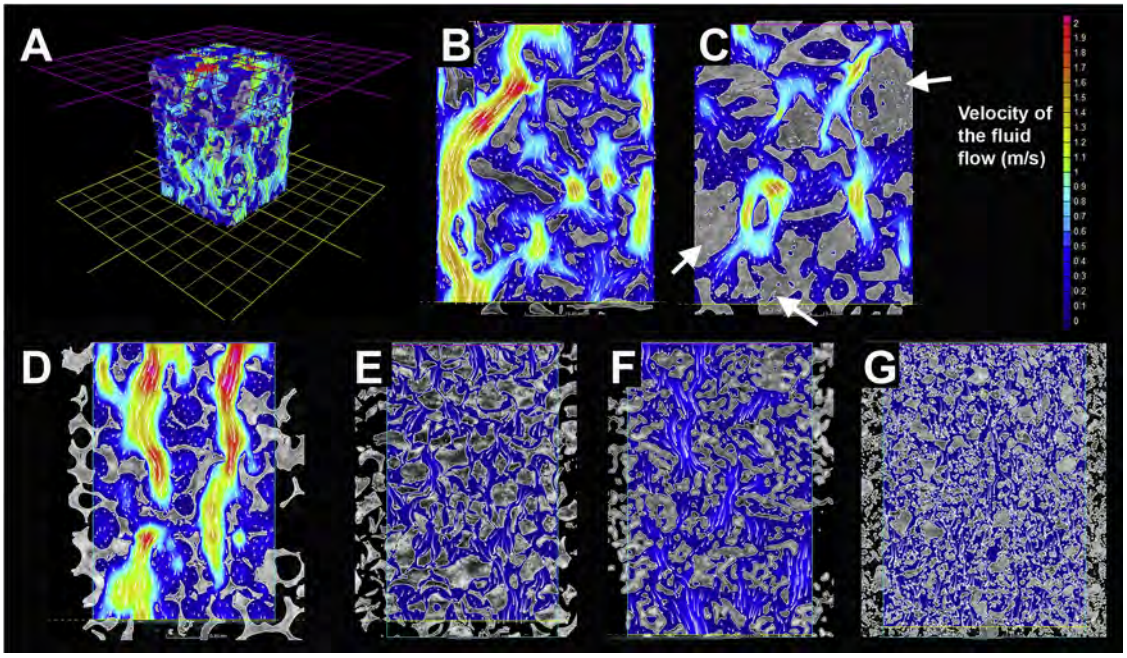

Fig. 2. Simulation of fluids dynamics. A) 3D analysis with the pink inlet plane and the parallel yellow outlet plane. B) 2D analysis of 1000-2000 µm of Osteopure ® granules. C) 2D analysis of Bio-Oss ® granules. The large granules of cortical bone markedly influence the velocity and the trajectory of the streamlines. D) 2D analysis of TCP dental HP ® 1000-2000 µm. E) 2D analysis of TCP dental HP ® 250-1000 µm granules, note that velocity is considerably reduced and the direction of streamlines appears more tortuous. F) 2D analysis of Biocoral ® granules, velocity is reduce and the trajectories are tortuous. G) 2D analysis of EthOss ® powder. Velocity is considerably reduced and the streamline trajectories are complexified by the numerous small particles that fragment the fluid flow. Velocity is color-coded according to the look-up-table from zero to 2 m/s; streamlines appear in white (For interpretation of the references to colour in this figure legend, the reader is referred to the web version of this article).

the sub-chondral bone had been grinded. Granules of this undecalcified purified hip were prepared with a bone miller (Roswitha P. Quétin, Dental-Products, Leimen, Germany) and they were sieved to obtain two groups of granules: 250 – 1000 µm (small) and 1000 – 2000 µm (large).

2.1.2. Bio-Oss ®

Granules of the undecalcified bovine xenograft Bio-Oss ®were directly purchased from Geistlich Pharma AG (Switzerland). The packaging and the leaflet package indicates they are prepared from bovine spongy bone which has been extensively deproteinized with a 300 °C treatment for 18 h (Kim et al., 2013). Granules (250 – 1000 µm and 1000 – 2000 µm of batches #81,600,947 and #81,600,788 respectively were used.

2.1.3. CopiOs ®

Granules of CopiOs ® (250 – 1000 µm and 1000 – 2000 µm) were directly purchased from Zimmer Dental (Germany). These granules are prepared by the Tutoplast process ® Tutogen Medical GmbH, Germany from bovine spongy bone, the process comprises alkali washes and oxidative treatments that preserve the organic and mineral parts of the bone matrix. Granules of batches # 13,517,185 and #20,108,414 were used.

2.1.4. TCP dental HP ®

These granules of the synthetic ceramic β-TCP (beta-tricalcium phosphate) are prepared by Kasios SAS by using the polyurethane foam technology as extensively reported elsewhere (Filmon et al., 2009; Schwartzwalder et al., 1963; Terranova et al., 2015). Granules (250 – 1000 µm and 1000 – 2000 µm) of batch #484/16.175 were used. They present a high porosity making them to resemble trabecular bone.

2.1.5. KeraOs ®

These granules of the synthetic ceramic are prepared by Keramat (A Coruña, Spain) in 250 – 1000 µm and 1000 – 2000 µm by a patented method. Granules of batches #1,115,121 12,007 were used. The packaging indicates that these granules are composed of β-TCP with a purity higher than 99 %.

2.1.6. TCH ®

These granules (250 – 1000 µm and 1000 – 2000 µm) are prepared by Kasios SAS with a slurry containing 25 % of β-TCP and 75 % of hydroxyapatite powder per 100 ml of water. Granules of batch #404/15.393 were used.

2.1.7. BioCoral 1000®

It was prepared by Biocoral France (Saint-Gonnery, France) by crushing the exoskeleton of natural coral into granules of 630 – 1000 µm.

2.1.8. EthOss®

EthOss® is a biphasic dry powder containing 35 % calcium sulfate and 65 % of calcium triphosphate. It is prepared by Medbone Medical Devices Lda, (Sintra, Portugal) for bone grafting and for stimulating bone regeneration. Batch #ETT0505530S lot 0000 was used from a gift from Dexter (Argenteuil, France).

2.1.9. Nanostim®

Nanostim® is a synthetic paste made of nanocrystalline hydroxyapatite in sterile water to produce a slurry; it is sold in disposable syringes. The product is prepared by Medtronic and a syringe ref. 8,470,050 was purchased from Medtronic France.

The molecular composition of all types of granules was verified on an InVia Qontor Raman microscope (data not shown) as previously reported (Arbez et al., 2019).

2.2. MicroCT analysis

MicroCT analysis was performed on a Skyscan 1172 microcomputed

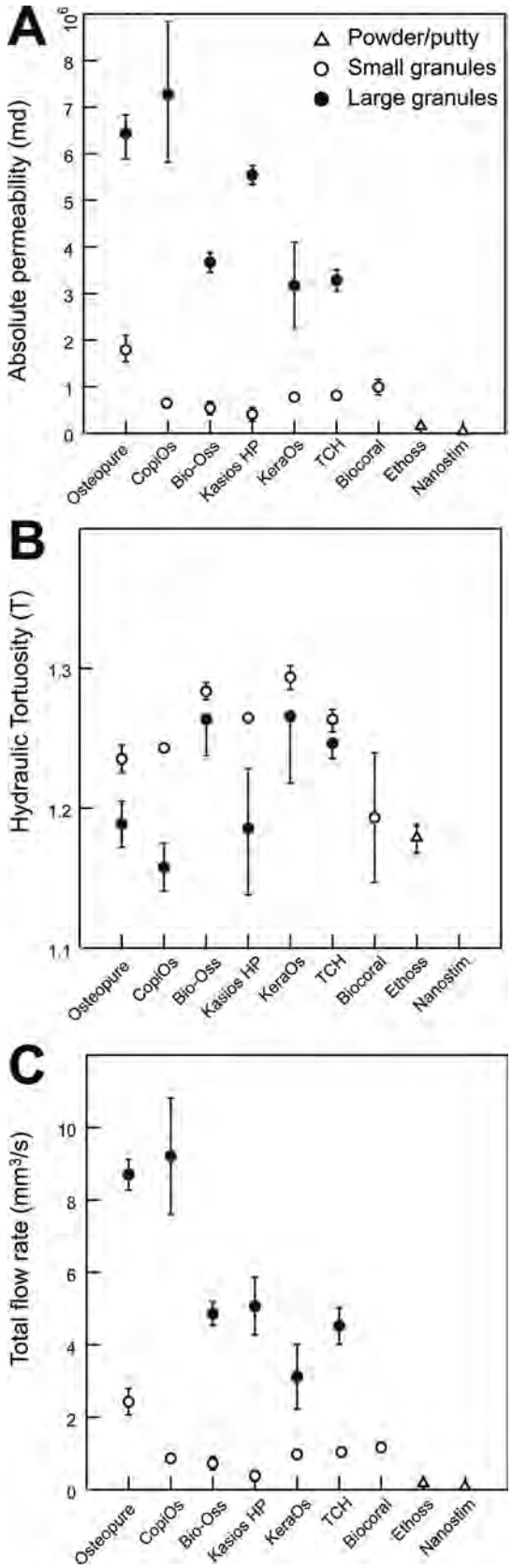

Fig. 3. Statistical and graphical analysis of fluid dynamics in a variety of granules stacks. Tortuosity could not be determined with Nanostim® because the flow rate across the putty was null. ●Large granules, ○ small granules, △ putty or powder biomaterials.

tomograph (Bruker microCT, Kontich, Belgium) as previously reported (Arbez et al., 2019). The different types of biomaterials were placed in Eppendorf polystyrene test tubes (10 mm in diameter) and gently agitated to allow the granules to settle and optimize their 3D spatial arrangement in the dry state; a volume of ~330 mm^3 was analyzed. Analysis was done in triplicate with the different granules stacks. The microCT was operated at 80 kV, 100 µA with a 0.5 mm aluminum filter. The cubic voxel size was fixed at 4.95 µm and the angular rotation step at 0.25°. Microarchitecture parameters were obtained with the CTAn software (Bruker) after thresholding of the pores (Tassani et al., 2014). They included measures of porosity (Po, in %), mean pore diameter (Po.Diam, in µm) and specific surface (representing the interface between bone or biomaterial and the porosity (Po.S/TV, in mm^2/mm^3, where Po.S is the whole pore surface and TV, the volume of interest as previously reported. The 3D models of each type of granules were obtained with VG Studiomax 3.2 (Volume Graphics GmbH, Heidelberg, Germany) operating in the volume-rendering mode.

2.3. Simulation of fluid dynamics

Simulation of fluid dynamics is also referred as Computational fluid dynamics (CFD). Once the 3D models were obtained, the add-on "Transport Phenomena Simulation" module of VG Studiomax was used to compute the computational fluid dynamics simulations across the different biomaterials (Rieth-Hoerst et al., 2014). The boundary conditions were set as follows: first, a superior plan was defined; then, a parallel opposite plane (separated by 2870 µm) was selected. The following parameters were used for simulation: an outlet pressure of 1 Pa; then, the wall boundaries were defined as sealed faces, the physical properties for the fluid dynamic viscosity was set at $\eta = 0.00155$ Pa.s (similar to that of extracellular fluids (Zarnitsyn and Fedorov, 2007)). Computation was done with a 3-voxel simulation cell size and 1000 iterations. The following parameters were obtained:

- Absolute permeability (k): it is a measure of the ability of a porous stack of granules to allow fluids to pass through it. The unit of measure is the milliDarcy (Fanchi, 2018; Mostaghimi et al., 2013).
- Hydraulic tortuosity (T): it is a parameter describing the average elongation of fluid streamlines in a porous medium as compared to a free flow (with a value = 1). Hydraulic tortuosity is a dimensionless quantity, but is always greater than one (Duda et al., 2011; Espinoza-Andaluz et al., 2017).
- Total flow rate: it Indicates the total volume of fluid per second transported through the volume of the pack of granules (Baker et al., 2015). The unit of measure is the mm^3/s.

In addition, the graphical analysis illustrates the calculated velocity distribution in color-coded way according to a LUT (look up table). The streamlines, overlaid in white, illustrate the direction of the flow between the granules.

2.4. Statistical analysis

Statistical analysis was performed using the Systat statistical software release 13.0 (Systat Software Inc., San José, CA). For each biomaterial considered, the mean of the three trials was considered. All data were expressed as mean ± standard error of the mean (SEM). Differences between the groups were sought with the Kruskall-Wallis non-parametric analysis of variance followed by the Conover-Inman test for all pairwise comparisons. Linear correlations between microarchitecture and fluid dynamics parameters were searched and the Pearson's coefficient of correlation was determined. A difference was considered as significant when $p < 0.05$.

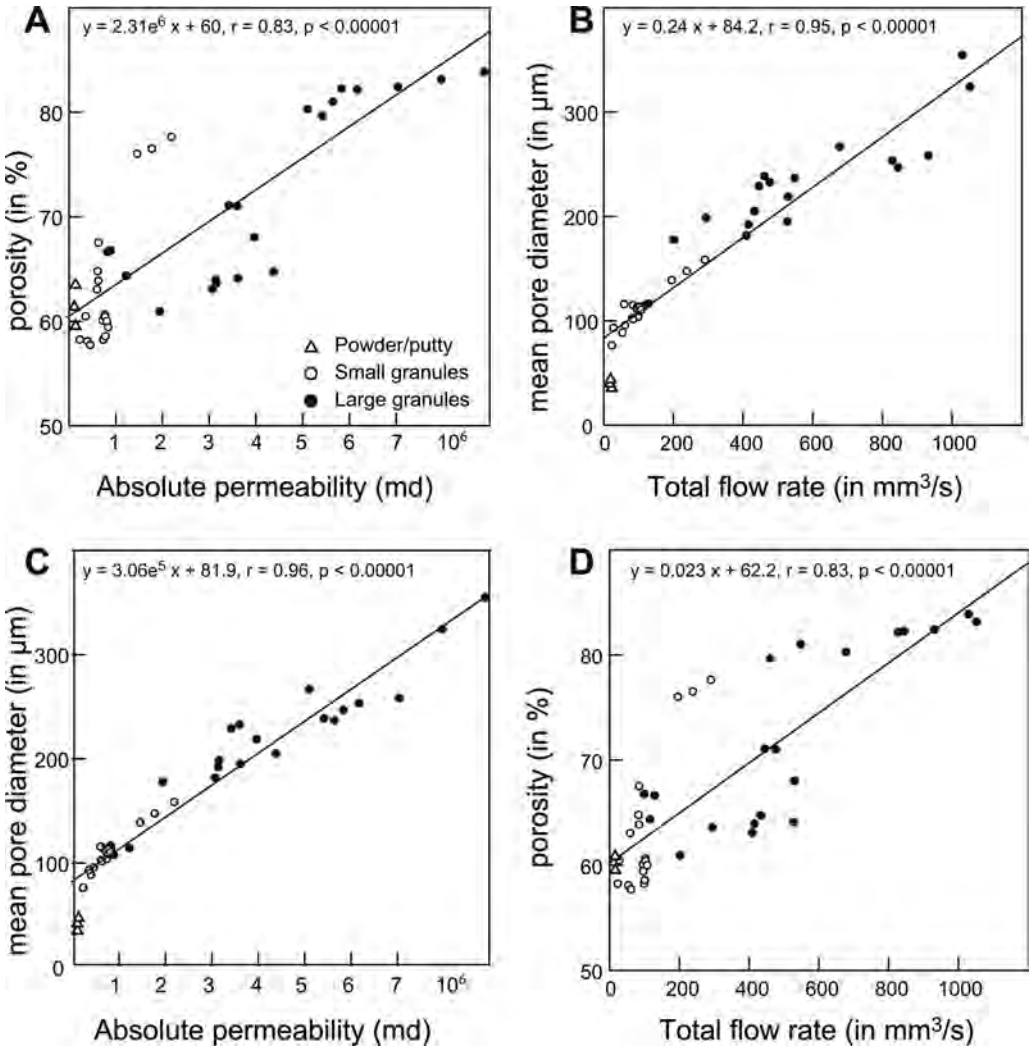

Fig. 4. Relationships between microarchitecture and fluid dynamics parameters. In all cases, the linear equation is mentioned.

3. Results

3.1. MicroCT analysis

The microCT analysis of the different scaffolds of biomaterials appears on Fig. 1 and the morphometric parameters are depicted in Table 1. For convenience, the two biomaterials composed of mineral granules (i.e., EthOss ® and Nanostim ®) are grouped together in the table and the graphs. The small granules (i.e. with a size < 1000 µm) constitute another group while all biomaterials with granules ranging from 1000 to 2000 µm constitutes the group of large granules. EthOss ® appeared as a powder composed of very small particles packed together and the diameter of the pore between these small granules was very reduced (Fig. 1A). The specific Po.S/TV was maximal for this material due to the high number of mineral granules. Nanostim ® appeared as a compact mass without a clearly defined porosity between the hydroxyapatite nanoparticles. The occasionally observed pores were in fact bubbles appearing during extrusion of the paste from the syringe. The biomaterial was heterogeneous, and packs of nanoparticles appear as white and poorly delimited masses on the microCT images (Fig. 1B). Stacks of small granules are composed of intermeshing granules with less porosity than stacks of large granules ((Fig. 1C-D). Granules of allogenic or xenogenic bone give stacks with an intermeshing of fragments of bone trabeculae (Fig. 1E-F). However, Bio-Oss ® appeared composed of a mixture of trabecular and cortical bone; these cortical fragments were easily identified by their largest size and the presence of Haversian canals (Fig. 1F). The synthetic ceramics created scaffolds mimicking the trabecular bone architecture because the networks have an interconnected porosity and the substance of the biomaterials creates connected structures when granules come in direct contact (Fig. 1G-H). For TCP dental HP ®, the interconnected porosity was clearly evidenced while closed and round pores were clearly identified in KeraOs ® (Fig. 1H). TCH ® and KeraOs ® were composed of large granules and presented the lowest porosity and pore diameter of this group.

3.2. Simulation of fluid dynamics

Fig. 2 illustrates the principle and results of the simulation of fluid dynamics applied to several stacks of granules. Fig. 2A illustrates the conditions of the simulation: the lateral walls of the volume of interest have been trimmed with a clipping box and defined as no-slip faces. The axis-flow is in the vertical direction starting from the pink inlet plane to the opposite plane in yellow that constitutes the outlet face. The calculated velocity of the fluid is color-coded according to the look-up-table that was the same for all analyses. The streamlines are also illustrated. The other pictures correspond to 2D images of different stacks of biomaterials. One can easily see that large granules favor the permeation of fluids through the scaffolds (Fig. 2A-D) while small granules induce a reduced velocity. It is noteworthy that the large particles of

cortical bone present in Bio-Oss ® affect the velocity and the trajectory of the fluids. The fluid dynamic parameters are illustrated on Fig. 3. Nanostim ® was very difficult to investigate with the permeation software, as almost no porosity was present in the samples. So absolute permeability and flow rate appeared null and the tortuosity could not be determined. On Fig. 3, the influence of the granule size was evidenced on all parameters. Stacks of small granules had significantly lowest absolute permeability and flow rate than the counterpart large granules ($p < 0.001$). On the contrary, the flowing routes were significantly increased because the trajectories of the streamlines were more complex and elongated.

Correlations between microarchitecture parameters and fluid dynamic parameters appear on Fig. 4. Absolute permeability was significantly correlated with porosity, mean pore diameter and specific surface. The total flow rate was also highly correlated with the mean pore diameter and porosity (Fig. 4). Tortuosity was negatively correlated with porosity ($r = -0.62$, $p < 0.0001$); correlation was also observed with mean pore diameter ($r = 0.36$, $p = 0.02$) but no correlation was found with Po.S/TV.

4. Discussion

In a material with an interconnected porosity, porosity is described as made of two phases: pores bodies connected by small canaliculi termed pore throats (Lindquist et al., 2000). The equation describing fluid flow in porous media is Darcy's Law (Armstrong et al., 2018; Darcy, 1856). The movement of a fluid through a porous sample depends on cross-sectional area of the sample, pressure difference, length of the flow path, and viscosity of the flowing fluid. The fluid flows from high pressure to low pressure. In the present study, the microarchitecture characteristics of the different types of granules were quantified by microcomputed tomography, a powerful tool to evaluate bone and porous materials such as foams, rocks and scaffolds (Ho and Hutmacher, 2006; Lapczyna et al., 2014; N'Diaye et al., 2013; Sasov and Van Dyck, 1998; Voltolini et al., 2011). However, morphometric analysis did not allow computing separately pore bodies from throats. In a recent paper, we analyzed the 3D characteristics of nine commercial biomaterials usable for bone grafting in maxillo-facial surgery (Arbez et al., 2019). Stacks of small granules ($250-1000$ µm) had a much lower porosity than their corresponding large granules ($1000-2000$ µm) as evidenced by several technics applied to microCT images (morphometry, histogram frequency of pore diameter and vector analysis of porosity). In addition, it was found that the pore bodies obtained with the small granules were smaller than the 300 µm commonly accepted size that favors vascular invasion in a grafted site. In the present study, we analyzed 15 different biomaterials with a small or large granulometry and added two types of putty. Putties (non-hardening pastes) are reported in the literature to be satisfactory for bone grafting (Bohner, 2010a; Callan et al., 2000; Neiva et al., 2008) but some reports provide negative results with bone non-union or poor bone regeneration (Kim et al., 2012; Kurien et al., 2013; Lee et al., 2009). The two putties analyzed in the present study had the lowest pore diameter and Nanostim® had almost no quantifiable porosity. Although bioactive glasses (calcium sodium phosphosilicate) are also sold by some companies for bone grafting and that a number of publications have been published (El-Rashidy et al., 2017; Gerhardt and Boccaccini, 2010), we did not use these biomaterials in the present study due to their health hazards. Silica and silicones have been recognized to induce an autoimmune response (see review by (Subra, 2004)), particles can migrate in the organism (Absher et al., 1992; Brown, 2009; Slavin et al., 1985), they can induce an acute renal failure in animals when implanted in bone or peritoneum (Gorustovich et al., 2007; Kawanabe et al., 1992) and recent findings indicate potential carcinogenicity (Dashevsky et al., 2019).

The physics of drainage of a fluid inside a porous material such as rock or sandstone is commonly explained by the invasion percolation theory (Berkowitz and Ewing, 1998). Simulation of fluid dynamics-CFD is a recently developed method used for evaluation of permeability of porous networks like the exploration studies done in the oil-gas industry and water drainage for soils (Armstrong and Berg, 2013; Armstrong et al., 2018; Bourbie and Zinszner, 1985; Hilpert and Miller, 2001). For biological tissues or biomaterial, permeability reflects the amount of fluid flow that can penetrate and diffuse through a porous scaffold (Widmer and Ferguson, 2013). A permeable scaffold is able to transmit nutrients and oxygen through its interconnected pores. The method has been applied to evaluate the permeability of the trabecular bone network (Basri et al., 2017; Daish et al., 2017; Egan et al., 2017; Sandino et al., 2014; Teo and Teoh, 2012; Widmer and Ferguson, 2013). To our knowledge, this study is the first attempt to simulate the body fluid drainage through stacks of granular materials usable for bone grafting. All different types of granules are used to fill the 3D space thus giving virtual scaffolds that mimic what happens when a surgeon fills a bone cavity (Guillaume, 2017; Ndiaye et al., 2015). The stacks of large granules presented the highest values for absolute permeability and total flow rate. The two putties had values close to, or equal to, zero, indicating that the access of body fluids inside the grafted area with such products will be considerably reduced. CFD studies have shown that permeability of trabecular bone is negatively correlated with the trabecular bone volume (BV/TV, according to the American Society for Bone and Mineral Research nomenclature which is defined as 100 - Po) and positively with trabecular separation (Tb.Sp, which correspond to Po.Diam measured here) (Sandino et al., 2014; Widmer and Ferguson, 2013). In the present study, absolute permeability and flow rate were also found positively correlated with porosity and with mean pore diameter. It should be noted that presence of cortical bone fragments mixed with trabecular bone granules present in BioOss® significantly modified the fluid dynamics by creating heterogeneous and sinuous paths. Hydraulic tortuosity is a parameter linked to microarchitecture that measures the complexity of the paths that a liquid follows through an interconnected porosity (Gommes et al., 2009; Solórzano et al., 2013). As expected, tortuosity was markedly increased with the small granules and impossible to compute for Nanostim®. The quantitative method used here is graphically illustrated and more easily computed than succolarity, a fractal parameter that cannot be adjusted with pressure and dynamic viscosity of the fluid (N'Diaye et al., 2013; Ndiaye et al., 2015).

5. Conclusion

Simulation of fluid dynamics-CFD is an interesting approach to evaluate bone biomaterials in pre-clinical steps (Basri et al., 2017). It confirms that accessibility of body fluids and progenitor cells can be completely different, depending on the shape and 3D arrangements of granules within a stack.

Declaration of Competing Interest

No conflicts of interest, financial or otherwise, are declared by the authors.

Acknowledgments

Mrs. N. Gaborit and S. Lemière are thanked for their technical help with microCT analysis.

Funding

This work was made possible by grants from ANR; program LabCom "NextBone".

References

Absher, M.P., Hemenway, D.R., Leslie, K.O., Trombley, L., Vacek, P., 1992. Intrathoracic distribution and transport of aerosolized silica in the rat. Exp. Lung Res. 18, 743–757.

Arbez, B., Libouban, H., 2017. Behavior of macrophage and osteoblast cell lines in contact with the beta-TCP biomaterial (beta-tricalcium phosphate). Morphologie 101, 154–163.

Arbez, B., Kun-Darbois, J.D., Convert, T., Guillaume, B., Mercier, P., Hubert, L., Chappard, D., 2019. Biomaterial granules used for filling bone defects constitute 3D scaffolds: porosity, microarchitecture and molecular composition analyzed by microCT and Raman microspectroscopy. J. Biomed. Mater. Res. B Appl. Biomater. 107B, 415–423.

Armstrong, R.T., Berg, S., 2013. Interfacial velocities and capillary pressure gradients during Haines jumps. J. Physical Review E 88, 043010.

Armstrong, R.T., McClure, J.E., Robins, V., Liu, Z., Arns, C.H., Schlüter, S., Berg, S., 2018. Porous media characterization using Minkowski functionals: theories, applications and future directions. J. Transport Porous Media 1–31.

Baker, R.O., Yarranton, H.W., Jensen, J.L., 2015. 7 - conventional core analysis–rock properties. In: Baker, R.O., Yarranton, H.W., Jensen, J.L. (Eds.), Practical Reservoir Engineering and Characterization. Gulf Professional Publishing / Elsevier, Cambridge, MA, pp. 197–237.

Basri, H., Nasution, J.D., Syahrom, A., Sulong, M.A., Saad, A.P., Prakoso, A.T., Aminin, F., 2017. The effect of flow rate characteristic on biodegradation of bone scaffold. Malaysian J. Fund. Appl. Sci. 13, 546–552.

Berkowitz, B., Ewing, R.P., 1998. Percolation theory and network modeling applications in soil physics. Surv. Geophys. 19, 23–72.

Blok, Y., Gravesteijn, F., Van Ruijven, L., Koolstra, J., 2013. Micro-architecture and mineralization of the human alveolar bone obtained with microCT. Arch. Oral Biol. 58, 621–627.

Bohner, M., 2010a. Design of ceramic-based cements and putties for bone graft substitution. Eur. Cell. Mater. 20, 3–10.

Bohner, M., 2010b. Resorbable biomaterials as bone graft substitutes. Mater. Today 13, 24–30.

Bourbie, T., Zinszner, B., 1985. Hydraulic and acoustic properties as a function of porosity in Fontainebleau sandstone. J. Geophys. Res. Solid Earth 90, 11524–11532.

Brown, T., 2009. Silica exposure, smoking, silicosis and lung cancer—complex interactions. Occup. Med. 59, 89–95.

Callan, D.P., Salkeld, S.L., Scarborough, N.J.Id., 2000. Histologic analysis of implant sites after grafting with demineralized bone matrix putty and sheets. J. Implant Dent. 9, 36–44.

Carvalho, A.L., Faria, P.E., Grisi, M.F., Souza, S.L., Taba, M.J., Palioto, D.B., Novaes, A.B., Fraga, A.F., Ozyegin, L.S., Oktar, F.N., Salata, L.A., 2007. Effects of granule size on the osteoconductivity of bovine and synthetic hydroxyapatite: a histologic and histometric study in dogs. J. Oral Implant. 33, 267–276.

Chappard, D., Baslé, M.-F., Legrand, E., Audran, M., 2008. Trabecular bone microarchitecture: a review. Morphologie 92, 162–170.

Chappard, D., Terranova, L., Mallet, R., Mercier, P., 2015. 3D porous architecture of stacks of beta-TCP granules compared with that of trabecular bone: a microCT, vector analysis, and compression study. Front. Endocrinol. 6, 161.

Daish, C., Blanchard, R., Gulati, K., Losic, D., Findlay, D., Harvie, D., Pivonka, P., 2017. Estimation of anisotropic permeability in trabecular bone based on microCT imaging and pore-scale fluid dynamics simulations. J. Bone Rep. Recomm. 6, 129–139.

Darcy, H., 1856. Les fontaines publiques de la ville de Dijon : exposition et application des principes à suivre et des formules à employer dans les questions de distribution d'eau. Victor Dalmont, Paris.

Dashevsky, B.Z., Gallagher, K.M., Grabenstetter, A., Cordeiro, P.G., Dogan, A., Morris, E.A., Horwitz, S.M., Sutton, E., 2019. Breast implant-associated anaplastic large cell lymphoma: Clinical and imaging findings at a large US cancer center. Breast J. 25, 69–74.

Duda, A., Koza, Z., Matyka, M., 2011. Hydraulic tortuosity in arbitrary porous media flow. Phys. Rev. E 84, 036319.

Egan, P.F., Gonella, V.C., Engensperger, M., Ferguson, S.J., Shea, K., 2017. Design and fabrication of 3D printed tissue scaffolds informed by mechanics and fluids simulations. ASME 2017 Int. Design Engin. Tech. Conf. Comput. Inform. Engin. Conf. Am. Soc. Mech. Engin. Dig. Coll 1–10.

El-Rashidy, A.A., Roether, J.A., Harhaus, L., Kneser, U., Boccaccini, A., 2017. Regenerating bone with bioactive glass scaffolds: a review of in vivo studies in bone defect models. Acta Biomater. 62, 1–28.

Espinoza-Andaluz, M., Andersson, M., Sundén, B., 2017. Computational time and domain size analysis of porous media flows using the lattice Boltzmann method. Comput. Math. Appl. 74, 26–34.

Fanchi, J.R., 2018. Rock-fluid interaction, chapter 5. In: Fanchi, J.R. (Ed.), Principles of Applied Reservoir Simulation, 4th edition. Gulf Professional Publishing / Elsevier, Cambridge, MA, pp. 81–99.

Farber, L., Tardos, G., Michaels, J.N., 2003. Use of X-ray tomography to study the porosity and morphology of granules. Powder Technol. 132, 57–63.

Filmon, R., Retailleau-Gaborit, N., Brossard, G., Grizon-Pascaretti, F., Baslé, M.F., Chappard, D., 2009. MicroCT and preparation of ß-TCP granular material by the polyurethane foam method. Image Anal. Stereol. 28, 103–112.

Gerhardt, L.-C., Boccaccini, A., 2010. Bioactive glass and glass-ceramic scaffolds for bone tissue engineering. Mater. Manag. Health Care 3, 3867–3910.

Gommes, C.J., Bons, A.J., Blacher, S., Dunsmuir, J.H., Tsou, A.H., 2009. Practical methods for measuring the tortuosity of porous materials from binary or gray-tone tomographic reconstructions. Am. Inst. Chem. Engin. J. 55, 2000–2012.

Gorustovich, A.A., Monserrat, A.J., Guglielmotti, M.B., Cabrini, R., 2007. Effects of intraosseous implantation of silica-based bioactive glass particles on rat kidney under experimental renal failure. J. Biomater. Appl. 21, 431–442.

Guillaume, B., 2017. Filling bone defects with beta-TCP in maxillofacial surgery: a review. Morphologie 101, 113–119.

Hernigou, P., Dubory, A., Pariat, J., Potage, D., Roubineau, F., Jammal, S., Flouzat Lachaniette, C.H., 2017. Beta-tricalcium phosphate for orthopedic reconstructions as an alternative to autogenous bone graft. Morphologie 101, 173–179.

Hilpert, M., Miller, C., 2001. Pore-morphology-based simulation of drainage in totally wetting porous media. Adv. Water Resour. 24, 243–255.

Ho, S.T., Hutmacher, D.W., 2006. A comparison of micro CT with other techniques used in the characterization of scaffolds. Biomaterials 27, 1362–1376.

Ibrahim, N., Parsa, A., Hassan, B., Van der Stelt, P., Wismeijer, D., 2013. Diagnostic imaging of trabecular bone microstructure for oral implants: a literature review. Radiol. 42, 20120075.

Karageorgiou, V., Kaplan, D., 2005. Porosity of 3D biomaterial scaffolds and osteogenesis. Biomaterials 26, 5474–5491.

Kawanabe, K., Yamamuro, T., Kotani, S., Nakamura, T., 1992. Acute nephrotoxicity as an adverse effect after intraperitoneal injection of massive amounts of bioactive ceramic powders in mice and rats. J. Biomed. Mater. Res. - Part A 26, 209–219.

Kim, D.M., Nevins, M., Camelo, M., Nevins, M.L., Schupbach, P., Rodrigues, V.S., Fiorellini, J.P., 2012. Human histologic evaluation of the use of the dental putty for bone formation in the maxillary sinus: case series. J. Oral Implantol. 38, 391–398.

Kim, Y., Nowzari, H., Rich, S.K., 2013. Risk of Prion Disease Transmission through Bovine-Derived Bone Substitutes: A Systematic Review. Clin. Implant Dent. Rel. Res. 15, 645–653.

Kim, Y.J., Henkin, J., research, r., 2015. Micro-computed tomography assessment of human alveolar bone: bone density and three-dimensional micro-architecture. Clin. Implant Dent. 17, 307–313.

Knabe, C., Koch, C., Rack, A., Stiller, M., 2008. Effect of β-tricalcium phosphate particles with varying porosity on osteogenesis after sinus floor augmentation in humans. Biomaterials 29, 2249–2258.

Kurien, T., Pearson, R.G., Scammell, B.E., 2013. Bone graft substitutes currently available in orthopaedic practice: the evidence for their use. Bone Joint J. 95-B, 583–597.

Lapczyna, H., Galea, L., Wust, S., Bohner, M., Jerban, S., Sweedy, A., Doebelin, N., van Garderen, N., Hofmann, S., Baroud, G., Muller, R., von Rechenberg, B., 2014. Effect of grain size and microporosity on the in vivo behaviour of beta-tricalcium phosphate scaffolds. Eur. Cell. Mater. 28, 299–319.

Lee, S.S., Jang, J.H., Kim, K.S., Yoo, Y.J., Kim, Y.S., Lee, S.K., 2009. Failure of bone regeneration after demineralized bone matrix allograft in human maxillary sinus floor elevation. Bas. Appl. Pathol. 2, 125–130.

Lindquist, W.B., Venkatarangan, A., Dunsmuir, J., Wong, Tf., 2000. Pore and throat size distributions measured from synchrotron X-ray tomographic images of Fontainebleau sandstones. J. Geophys. Res. Solid Earth 105, 21509–21527.

Mastrogiacomo, M., Scaglione, S., Martinetti, R., Dolcini, L., Beltrame, F., Cancedda, R., Quarto, R., 2006. Role of scaffold internal structure on in vivo bone formation in macroporous calcium phosphate bioceramics. Biomaterials 27, 3230–3237.

Mostaghimi, P., Blunt, M.J., Bijeljic, B., 2013. Computations of absolute permeability on micro-CT images. Math. Geosci. 45, 103–125.

N'Diaye, M., Degeratu, C., Bouler, J.M., Chappard, D., 2013. Biomaterial porosity determined by fractal dimensions, succolarity and lacunarity on microcomputed tomographic images. Mater. Sci. Eng. C Mater. Biol. Appl. 33, 2025–2030.

Ndiaye, M., Terranova, L., Mallet, R., Mabilleau, G., Chappard, D., 2015. Three-dimensional arrangement of beta-tricalcium phosphate granules evaluated by microcomputed tomography and fractal analysis. Acta Biomater. 11, 404–411.

Neiva, R.F., Tsao, Y.P., Eber, R., Shotwell, J., Billy, E., Wang, H.L., 2008. Effects of a putty-form hydroxyapatite matrix combined with the synthetic cell-binding peptide P-15 on alveolar ridge preservation. J. Periodontol. 79, 291–299.

Ochoa, I., Sanz-Herrera, J.A., Garcia-Aznar, J.M., Doblare, M., Yunos, D.M., Boccaccini, A.R., 2009. Permeability evaluation of 45S5 Bioglass-based scaffolds for bone tissue engineering. J. Biomech. 42, 257–260.

Redondo, L.M., García Cantera, J.M., Hernández, A.V., Puerta, C.V., 1995. Effect of particulate porous hydroxyapatite on osteoinduction of demineralized bone autografts in experimental reconstruction of the rat mandible. Int. J. Oral Maxillofac. Surg. 24, 445–448.

Rieth-Hoerst, S., Reinhart, C., Günther, T., Dierig, T., Fieres, J., 2014. Methods to ensure accuracy and reliability of analyses and measurements done on CT data-sets. Proc. 11th Eur. Conf. on Non-Destructive Testing.

Sandino, C., Kroliczek, P., McErlain, D.D., Boyd, S.K., 2014. Predicting the permeability of trabecular bone by micro-computed tomography and finite element modeling. J. Biomech. 47, 3129–3134.

Sasov, A., Van Dyck, D., 1998. Desktop X-ray microscopy and microtomography. J. Microsc. 191, 151–158.

Schwartzwalder, K., Somers, H. and Somers, A.V., 1963. Method of making porous ceramics., US patent.

Slavin, R.E., Swedo, J.L., Brandes, D., Gonzalez-Vitale, J.C., Osornio-Vargas, A., 1985. Extrapulmonary silicosis: a clinical, morphologic, and ultrastructural study. Hum. Pathol. 16, 393–412.

Solórzano, E., Pardo-Alonso, S., Brabant, L., Vicente, J., Van Hoorebeke, L., Rodriguez-Perez, M., 2013. Computational approaches for tortuosity determination in 3D structures. 1St Int. Conf. Tomography of Materials and Structures (ICTMS 2013) 71–74.

Subra, J.-F.J., 2004. Silice et auto-immunité. Rev. Franc. Lab. 2004, 23–25.

Syahrom, A., Abdul Kadir, M.R., Abdullah, J., Ochsner, A., 2013. Permeability studies of artificial and natural cancellous bone structures. Med. Eng. Phys. 35, 792–799.

Tanaka, T., Komaki, H., Chazono, M., Kitasato, S., Kakuta, A., Akiyama, S., Marumo, K., 2017. Basic research and clinical application of beta-tricalcium phosphate (beta-

TCP). Morphologie 101, 164–172.
Tassani, S., Korfiatis, V., Matsopoulos, G., 2014. Influence of segmentation on micro-CT images of trabecular bone. J. Microsc. 256, 75–81.
Teo, J.C., Teoh, S.H., 2012. Permeability study of vertebral cancellous bone using micro-computational fluid dynamics. J. Comput. Meth. Biomech. 15, 417–423.
Terranova, L., Libouban, H., Mallet, R., Chappard, D., 2015. Analysis of beta-tricalcium phosphate granules prepared with different formulations by nano-computed tomography and scanning electron microscopy. J. Artif. Organs 18, 338–345.
Turunen, M.J., Prantner, V., Jurvelin, J.S., Kröger, H., Isaksson, H., 2013. Composition and microarchitecture of human trabecular bone change with age and differ between anatomical locations. Bone Miner. 54, 118–125.
van Lenthe, G.H., Hagenmuller, H., Bohner, M., Hollister, S.J., Meinel, L., Muller, R., 2007v. Nondestructive micro-computed tomography for biological imaging and quantification of scaffold-bone interaction in vivo. Biomaterials 28, 2479–2490.
Voltolini, M., Zandomeneghi, D., Mancini, L., Polacci, M., 2011. Texture analysis of volcanic rock samples: quantitative study of crystals and vesicles shape preferred orientation from X-ray microtomography data. J. Volcanol. Geotherm. Res. 202, 83–95.
Widmer, R.P., Ferguson, S.J., 2013. On the interrelationship of permeability and structural parameters of vertebral trabecular bone: a parametric computational study. Comput. Methods Biomech. Biomed. Eng. Imaging Vis. 16, 908–922.
Zarnitsyn, V.G., Fedorov, A.G., 2007. Mechanosensing using drag force for imaging soft biological membranes. Langmuir 23, 6245–6251.